Structural Response of Thin Cylindrical Shells Subjected to Impulsive External Loads

Steven W. Kirkpatrick* and Bayard S. Holmes†
SRI International, Menlo Park, California

Thin aluminum cylindrical rings and shells were subjected to impulsive external loads applied with explosives. Experimentally observed structural response mechanisms consisted of dynamic pulse buckling and large inward deflections of the loaded side of the shell. This structural response was analyzed with the DYNA3D finite-element code. Finite-element modeling of the response required modeling of initial imperfections in the geometry of the rings and shells and modeling of imperfections in the load in order to reproduce the observed buckling response. The effects of finite-element mesh refinement, initial imperfection amplitude, and imperfections in load are investigated. Methods for obtaining good solutions to this pulse buckling problem with finite-element codes have been noted.

Introduction

WHEN a cylindrical thin shell is subjected to an external impulsive load, the resultant inward motion of the shell increases compressive hoop stresses in the shell and can cause buckling. This pulse buckling is precipitated by an amplification of initial imperfections in the shell geometry, irregularities in shell material properties, or irregularities in the load. Previous theoretical and experimental work[1] concentrated on the onset of buckling and determining the threshold loads needed to produce buckling. The relationship between impulse and damage beyond the threshold load was determined mostly by experiment. Because the displacements associated with threshold pulse buckling are small, the governing equations can be linearized and more easily solved. Reference 1 lists a large body of theoretical work on the pulse buckling of cylindrical shells and other structures treated in this manner.

We performed experiments on ring structures and cylindrical shells made from 6061-T6 aluminum. Both structures had a thickness of 0.635 mm and a radius of 152.4 mm giving a radius-to-thickness ratio of 240. The shell structures had a length-to-diameter ratio of 1/2 with fixed ends. The experiments used impulse intensities three to four times greater than those required to produce threshold buckling. At these high load levels, the shell response includes large displacements and rotations, and the loaded side of the shell becomes significantly indented, producing large axial strains. At high enough loads, the axial stretching results in a circumferential fracture at the shell midplane.

We used the DYNA3D computer code developed at Lawrence Livermore National Laboratory[2] in the analysis of shell response. Recently, a variation of the Hughes-Liu shell element[3] was implemented into DYNA3D.[4] As implemented in DYNA3D, this is a four-node element with single-point integration and hourglass viscosity. The Hughes-Liu element offers the advantage of allowing a time step size that is insensitive to shell thickness and larger than that for corresponding brick elements. This feature permits more economical solutions and is important in applications where many elements are required for a good solution, as here.

Received Oct. 21, 1986; revision received Feb. 24, 1987.

*Research Engineer, Poulter Laboratory, Physical Sciences Division. Member AIAA.

†Senior Research Engineer, Poulter Laboratory, Physical Sciences Division.

In the following, we first review some past work on related buckling of shells. This work shows how buckling response is influenced by shell material properties and geometry as well as load characteristics. We then describe the experimental technique used to load the shells and the results of the experiments. The responses of the rings and the shells have features that can be seen in many structural impact and blast loading applications. Finally, the finite-element code is used to study the buckling response. This application shows the importance of element size and initial geometry in obtaining good solutions. Furthermore, the solutions shed light on the nature of the response that previous analytical solutions of the linearized shell equations could not show. Recommendations are made for structural response calculations within this class of pulse buckling problems.

Background

Dynamic buckling processes are different from static buckling problems in that the buckling depends on load history as well as load magnitude. The dependence arises because buckling results from the growth of initial imperfections in the structure in response to the applied load, which for a time exceeds the static load required to cause buckling. In general, the imperfections exist at all wavelengths, and the applied load is sufficient to cause the growth of many wavelengths at once. Although shorter wavelengths can grow faster, the load may exceed the static buckling load for these wavelengths for a shorter time. The final shape of the structure, which depends to a great extent on the buckle wavelength, thus depends on the competing growth of many buckle patterns.

Past analytical solutions for cylindrical shells under an external impulsive load first sought to find the threshold impulse that would produce buckling and the most amplified wavelength for the load. Solutions were obtained by assuming that the inward motion of the shell and the compressive hoop stresses were independent of the buckle growth. In addition, the solutions did not include the nonlinear effects of strain rate reversal as buckles grew large. For thick aluminum shells with radius-to-thickness ratios (a/h) of less than 100, the compressive stresses become large enough to cause the material to yield before it can buckle. Abrahamson and Goodier[5] derived equations for the buckling of these shells in which the buckling response is governed by the tangent modulus of the material. For very thin shells [$a/h > 400$], the buckling occurs while the material is still elastic. Goodier and McIvor[6] first derived the equations of elastic stability for these shells, and Lindberg[7] applied their equations to the problem of dynamic pulse buck-

ling. Lindberg also solved the equations for buckling of intermediate and thin shells [$100 < a/h < 400$], in which the material response is described by a varying tangent modulus. The effect of transient external pressures where the duration of the pressure pulse is no longer small in comparison with the structural response time was investigated by Anderson and Lindberg.[8] All of these solutions predicted the critical loads for pulsed buckling fairly well but not the response beyond the initial buckling. For all but the thick-shell analysis, experimentally observed mode numbers were lower than predicted.

The aforementioned solutions are based on the amplification of initial imperfections, which must be known a priori. In their formulation of the equations for plastic flow buckling, Abrahamson and Goodier noted that imperfections in shell geometry, material properties, and initial inward velocity of the shell could all influence the buckling. For simplicity of analysis, they treated imperfections in velocity resulting from nonuniform load application only. Anderson and Lindberg[8] later showed that the effect of radial shape imperfections would supersede the effect of velocity imperfections on pulse buckling of a thin aluminum shell if the magnitudes of the radial imperfections as a fraction of the wall thickness were comparable to the magnitudes of the velocity perturbations as a fraction of the initial velocity.

In this study, we are concerned with the response of thin shells with a radius-to-thickness ratio (a/h) of 240 at load levels well above the buckling threshold. The test cylinders were impulsively loaded over the front face of the shell. The load was cosine in distribution from -90 to $+90$ deg with the maximum load at the zero-degree position. Under these conditions, the buckling on the loaded side of the shell is similar to the uniform buckling produced by an axisymmetric impulse, but the buckling impulse threshold is increased. The increase ranges from 20% for plastic flow buckling of thick shells to 100% for elastic buckling of very thin shells.[1]

Experiments

In all our experiments, loads were produced using the spray lead at target (SPLAT) impulse simulation technique,[9] in which the load is produced by the impact of a spray of lead particles created by the detonation of an array of mild detonating fuses (MDF). MDF consists of a lead sheath over a core of PETN explosive and closely resembles rosin-core solder. The cosine impulse distribution is produced by varying the standoff and spacing of the MDF strands around the loaded side of the test cylinder. In any given experiment, the magnitude of the load is known to within $\pm 10\%$. Figure 1 shows the distribution of strands used to obtain the cosine load in the shell experiment.

A test ring and shell were made from 6061-T6 aluminum sheet stock rolled and welded into 30.5-cm diam cylinders. The sheet stock was 0.635 mm thick, resulting in a radius-to-thickness ratio for the test cylinders of 240. The ring had a length of 5.1 cm and the shell had an overall length of 25.4 cm. The cylindrical shell was welded over heavy end rings, which were 5.1 cm wide, giving an unsupported test length of 15.2 cm. The shell was bolted into a heavy steel test frame to obtain a fixed boundary condition at both ends.

The early-time buckling response was studied first using the ring. The load on the ring was cosine in distribution with an amplitude of 120 (± 12) Pa-s. An axial-view flash x-ray photograph of the ring was taken at 120 μs after load application to look at the buckled shape of the ring while the displacements were small. The deformed shape of the ring at 120 μs is shown in Fig. 2. The early-time response of the ring shows a relatively uniform buckling pattern on the loaded side of the ring with a mode number of approximately 50. The peak-to-peak displacements of the buckles vary between 1 and 3 mm.

In the shell experiment, the load was increased to a peak impulse intensity of 210 (± 21) Pa-s. High-speed movies were taken of the shell to show its overall response, and strain gages were placed on the inside of the loaded side of the shell. The output of the gage measuring the axial strain at the center of the loaded side of the shell is compared later with analytically predicted strain. The final deformed shape of the shell is shown in Fig. 3. Pulse buckling is evident on the front face of the shell with the predominant mode numbers between 35 and 40. Table 1 gives the dominant buckling mode numbers, the average inward deflection at the midplane, the buckle amplitude, and the

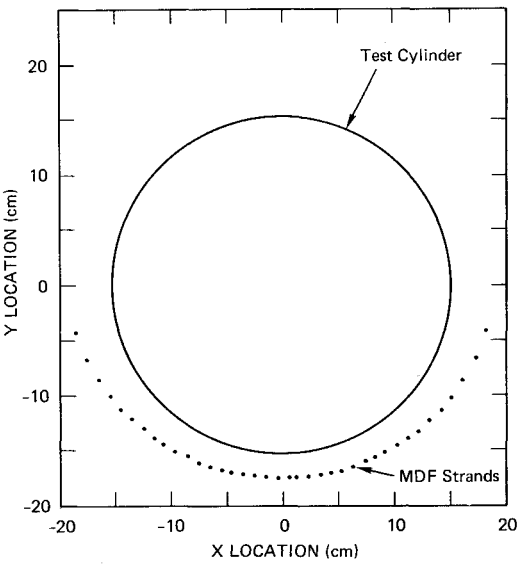

Fig. 1 Distribution of MDF strands.

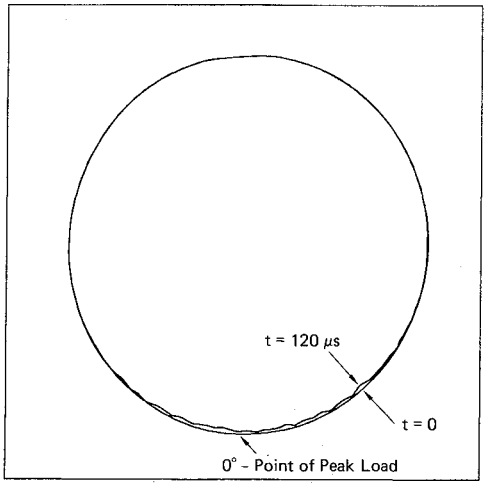

Fig. 2 Ring displacements measured with flash x-ray.

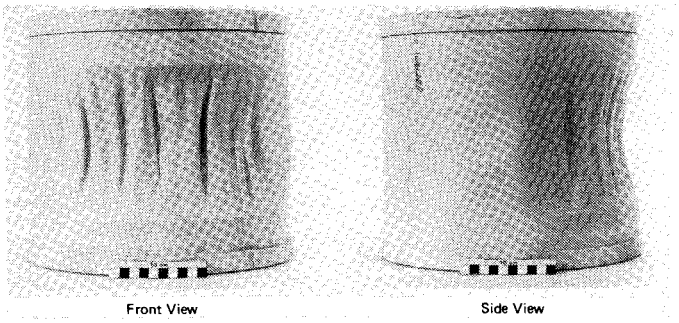

Fig. 3 Deformed shape of experimental shell.

Table 1 Comparisons of measured and calculated shell response[a]

Parameter	Experiment	Calculations		
		Idealized shape imperfections only	Measured shape imperfections only	Measured shape imperfections with estimated load imperfections
Dominant mode no.	35–40	35–40	35–40	35–40
Average deflection, mm	22	20	16	19
Buckle amplitude, mm	10	6	5	6
Maximum deflection, mm	28	24	19	22
Axial strain, %	1.5–7.2[b]	1–9	1–7	1–8

[a]Values at shell midplane near 0 deg. [b]Measured at discrete locations.

measured maximum inward deflection of the shell. The axial strain history at the shell midplane along the 0 deg position was measured with a strain gage, and the peak axial strain recorded at that position was 5.7%. Other axial strain measurements made with surface markings ranged from 1.5 to 7.2%. Inspection of the strain measurements showed that the magnitude of the axial strain varies a great deal with respect to the buckle pattern, with the largest strains along a crest of an inward buckle. Because of this variability, the magnitude of the measured axial strain is influenced by the position of the strain gage.

Imperfection Measurement and Idealization

The initial shape imperfections in the shell must be included in the finite-element mesh to reproduce the buckling response.[10] Two sets of imperfection distributions are used in calculations presented here. The first set is based on past measurements of the imperfections in thin shells. This set is idealized in that it is generated by a simple algorithm and has the generic characteristics of imperfections found in most thin shells. The purpose of this idealized imperfection algorithm is to provide a general format that can be used in calculations without making detailed measurements on the particular shell being analyzed. The second set of imperfections was that measured on the shell.

Idealized Shape Imperfections

Measurements of shape imperfections in cylindrical shells have been made to supplement buckling analyses.[11,12] The form of the imperfections measured in these studies depends on the manufacturing process, but the imperfections in most shells have similar characteristics. In particular, the predominant imperfections form ridges along the length of the shell. At the lower mode numbers, these ridges run the entire length of the shell. In addition, the modal amplitude of the imperfections decreases with increasing mode number.

From the data in Ref. 12 on cylindrical aerospace shell structures several feet in diameter, we assumed an idealized exponential distribution in amplitude that fits much of the available data. In addition, we assumed that the phase angle of the modal contribution ϕ_n was a random variable. These assumptions led to the following idealized form for shape imperfections in our initial calculations:

$$\Delta R(\theta) = \sum_{n=2}^{N} A_n \cos(n\theta + \phi_n) \tag{1a}$$

with

$$A_n = 0.05h \quad (n \leq 10)$$
$$= h/n^{1.3} \quad (n > 10) \tag{1b}$$

where ΔR is the error in radius, N the highest mode number included in the characterization, n the mode number, A_n the modal amplitude, ϕ_n the random phase angle of mode n, and h the shell thickness. Note that the amplitude of modes below 10 is held constant to limit the magnitude of ΔR. This is in keeping with much of the available data. Furthermore, because these modes do not contribute to the buckling process studied here, their absolute magnitude does not affect the results of our calculations.

Most of the calculations in this paper use this so-called idealized form of geometric imperfection. In these calculations, the highest mode number included was 200, and values of ΔR at nodes of the finite-element mesh were generated using a random number algorithm to find the corresponding ϕ_n.

Measured Shape Imperfections

In addition to estimating shape imperfections in the ring and shell from past measurements, we measured the shape imperfections in the shell before testing. We mounted the shell on a modified lathe bed with a potentiometer to measure the angular position of the shell and a linear voltage displacement transducer (LVDT) to measure the radial position of the shell surface. Output from the LVDT was recorded on a digital oscilloscope while the shell was rotated at a constant angular velocity. Approximately 1800 data points were obtained around the shell, and this measurement was repeated at 31 evenly spaced axial locations. Figure 4 shows a three-dimensional plot of the initial imperfections measured on a shell.

The distribution of the idealized imperfections was compared with the measured distribution using a fast Fourier transform (FFT) technique. For the estimated imperfections, the amplitude of the modal imperfections is simply the A_n. For comparison, an FFT of the measured imperfections at the shell midplane was performed to obtain the amplitude of the modal imperfections. The transformation required recasting the data into 1024 (2^{10}) points using linear interpolation. Figure 5 shows both the idealized imperfection distribution (A_n) and the Fourier coefficients approximated by the FFT for the measured imperfections. In Fig. 5, the coefficients are connected with continuous curves to facilitate comparison. The amplitude of the idealized imperfections appears to be a good approximation to the measured imperfections at the lower mode numbers, but above a mode number of 15, the amplitude of the measured imperfections drops off much more quickly than the idealized imperfections. The amplitude of the measured imperfections are lower than the idealized imperfection by a factor of 4 at a mode number of 25 and by nearly an order of magnitude at a mode number of 50. This is probably an effect of the small scale of the shells tested here in contrast to the large shells used to form the data base in Ref. 12.

Load Imperfections

The array of MDF providing the load in the experiments is designed to produce a smooth, nearly cosine load without any ripples. Imperfections in the load distribution can be caused by the ripple introduced by each individual strand, nonuniformity

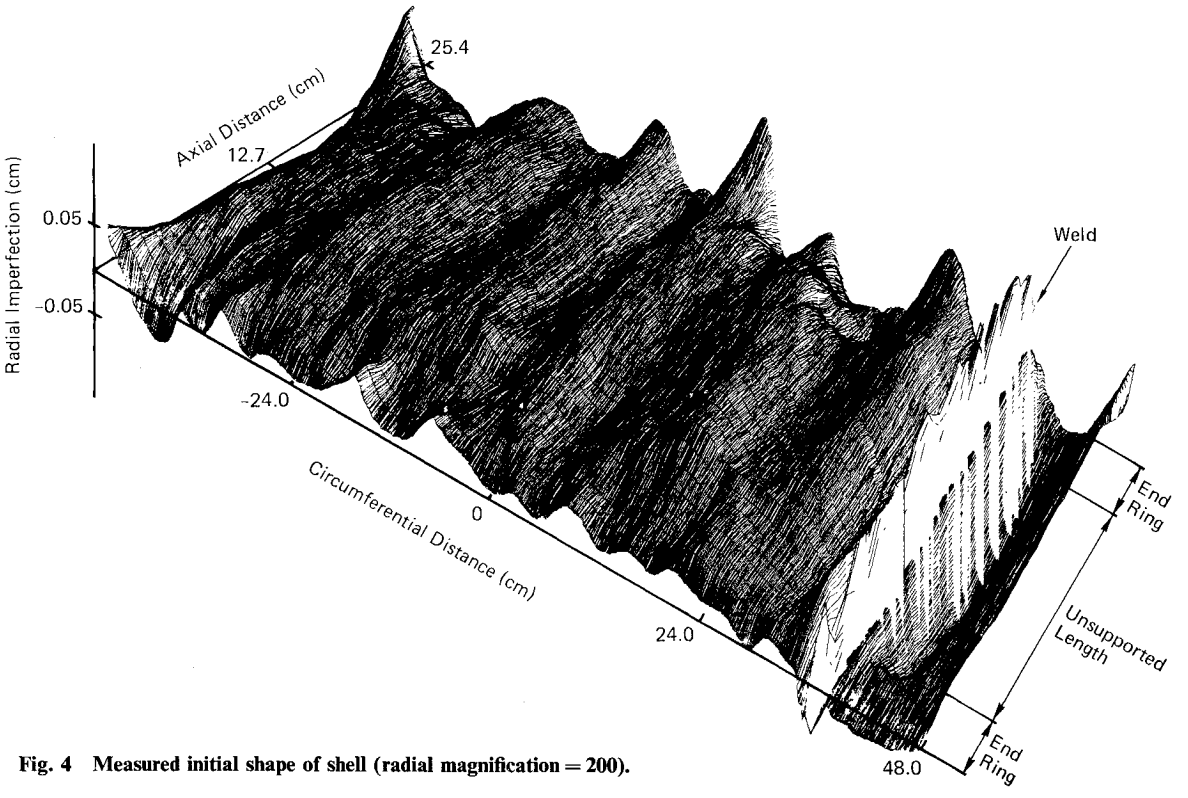

Fig. 4 Measured initial shape of shell (radial magnification = 200).

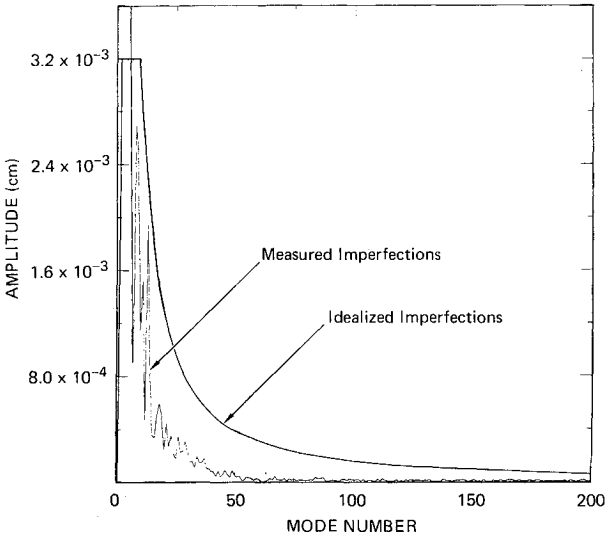

Fig. 5 Modal composition of imperfections.

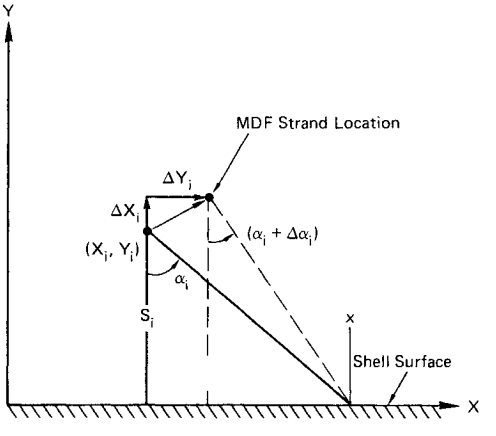

Fig. 6 MDF geometry.

of the MDF strands, and imperfections in the locations of the strands in the experimental setup. Previous analysis of the SPLAT technique[9] investigated the ripple in the load resulting from the individual MDF strands, under the assumption that each strand was perfectly placed. It was shown that making the standoff distance of the MDF array greater than twice the spacing between the strands made the ripple negligibly small if the strands were perfectly placed. For example, an infinite flat array with a standoff-to-spacing ratio of 2.0 has a theoretical ripple of less than 0.01% of the impulse delivered. However, in practice, the array positions of the MDF strands deviate slightly from their ideal design locations and the ripple in the load is much larger.

To estimate the effect of location errors, we calculated the impulse distribution on the shell surface from each strand in the MDF array and then summed the contribution of all the strands. The geometry of this problem is shown in Fig. 6. From Ref. 9, the normal impulse intensity delivered at a given position on the shell x from the ith MDF strand located at X_i, Y_i is

$$I_i(x) = \frac{mV}{2\pi S_i} \cos^3\alpha_i \tag{2}$$

where m is the total mass of lead per unit length of MDF, V the uniform velocity of the expanding spray of lead, S_i the standoff distance of the MDF strand from the shell, and α_i the angle of obliquity shown in Fig. 6. The total impulse delivered can be found by summing the contributions of each strand[9]

$$I(x) = \sum_{i=1}^{P} \frac{mV}{2\pi S_i} \cos^3\alpha_i \tag{3}$$

where P is the total number of strands.

The fractional change in the total impulse is found by taking the derivative of Eq. (3) with respect to S_i and α_i:

$$\frac{\Delta I(x)}{I(x)} \cong \left[-\sum_{i=1}^{P} \left(\frac{3\cos^2\alpha_i \sin\alpha_i \, \Delta\alpha_i}{S_i} + \cos^3\alpha_i \frac{\Delta S_i}{S_i^2} \right) \right] \Bigg/ \sum_{i=1}^{P} \frac{\cos^3\alpha_i}{S_i} \tag{4}$$

The changes in α_i and S_i resulting from the deviations in the strand locations ΔX and ΔY are found from the problem geometry as

$$\Delta S_i = \Delta Y \tag{5}$$

$$\Delta\alpha_i \cong \tan^{-1}\left(\frac{-S_i \, \Delta X_i - (x - X_i) \, \Delta Y_i}{(x - X_i)^2 + S_i^2} \right) \tag{6}$$

The strand location errors ΔX_i and ΔY_i are assumed to be independent and random with a normal distribution. The distribution of strand locations in actual arrays was measured from photographs of the arrays. A normal distribution of displacements with a standard deviation of 1.5 mm was found to be a good approximation of the errors in strand location.

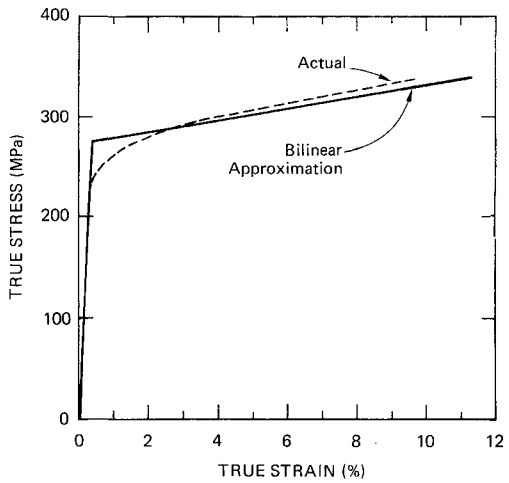

Fig. 7 Measured stress-strain curve for simple tension and bilinear approximation.

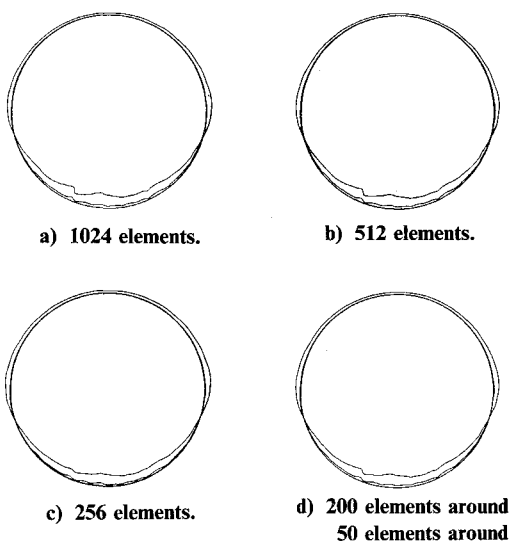

a) 1024 elements. b) 512 elements.

c) 256 elements. d) 200 elements around front, 50 elements around back.

Fig. 8 Effect of mesh refinement. Deformed shapes shown at 120 and 600 μs.

The load imperfections were introduced into the finite-element calculations by numerically generating a set of random normal strand displacements with a standard deviation of 1.5 mm. This random set of strand displacements was then used with Eq. (4) to give the fractional change in the load level at each nodal location. The maximum fractional imperfection in the load distribution in these calculations was 5.1%. The dominant mode number of the load imperfections is approximately 20.

Finite-Element Analysis

The finite-element calculations were performed using the DYNA3D computer code developed at Lawrence Livermore National Laboratory.[2] DYNA3D is an explicit three-dimensional finite-element code for analyzing the large deformation dynamic response of solids and structures. The equations of motion are integrated in time using the central difference method. Spatial discretization was achieved using four-node Hughes-Liu[3] shell elements. These elements use a reduced integration with an hourglass viscosity to control zero-energy modes as implemented by Hallquist, Benson, and Goudreau.[4]

The material model used in these calculations is an elastic-plastic model with a Mises yield function and associated flow rule and combined linear isotropic/kinematic hardening.[13] A combination of 20% isotropic and 80% kinematic hardening was chosen based on past experimental work on 6061-T6 aluminum structures. A parameter study showed that the effect of the proportion of isotropic and kinematic hardening was small.

Parameters for the bilinear model used in the calculations were based on quasistatic tensile tests of the material used in the shell and ring construction. These tests showed that the rolled sheet stock used in the shell and ring constructions was nearly isotropic in the plane of the sheet. Figure 7 compares the measured true stress-strain curve for the material and the bilinear approximation used in the finite-element calculations. Some compromise was made in modeling the material near the yield point to provide a good overall fit to the experimental data.

Mesh Refinement

The dynamic pulse buckling in the ring and shell experiments occurs at mode numbers between 35 and 50 on the loaded side of the shell. Because of the short wavelength of these buckles, a fine mesh around the circumference of the shell is required to model the buckling response properly. To minimize the elements required for the three-dimensional shell calculation, we first performed a mesh refinement study on a model of the ring experiments. The finite-element model of the ring consisted of a single circular row of shell elements constrained to plane strain along the ring axis. For each calculation, the load was cosine in distribution with a peak impulse intensity of 120 Pa-s. Ring models were generated with 1024, 512, and 256 elements uniformly distributed around the circumference. Each formulation included the idealized random imperfections in the radius of the ring in order to precipitate buckling.

The effect of mesh refinement is shown in Fig. 8, where the predicted ring shapes at 120 and 600 μs are plotted for the 1024, 512, and 256 element rings (Figs. 8a–8c). Visual examination of the three calculations shows little difference between the 512- and 1024-element calculations, but a significant loss in the details of response in the 256-element calculation.

Because the buckling occurs only on the loaded side of the ring, a fourth model was generated that has 200 elements across the loaded half of the ring and 50 elements around the back half. This mesh gives a finer resolution in the region of the buckling and uses fewer elements on the back where there is less bending response. The deformed shape of this mesh at 120 and 600 μs is shown in Fig. 8d. This fourth mesh reduces the total number of elements in the ring to 250, but maintains approximately 8 to 10 elements per buckle wavelength on the front of the shell. The predicted response from this mesh is

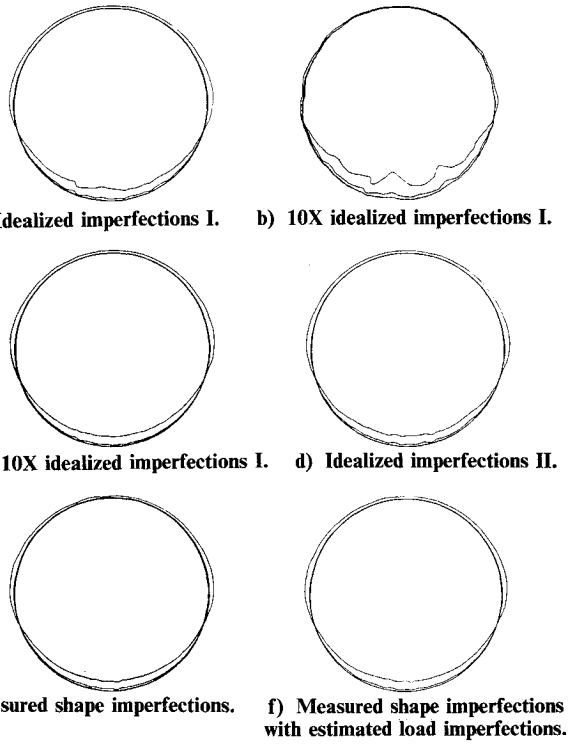

a) Idealized imperfections I. b) 10X idealized imperfections I.

c) 1/10X idealized imperfections I. d) Idealized imperfections II.

e) Measured shape imperfections. f) Measured shape imperfections with estimated load imperfections.

Fig. 9 Sensitivity of buckling response to initial imperfections. Deformed shapes shown at 120 and 600 μs.

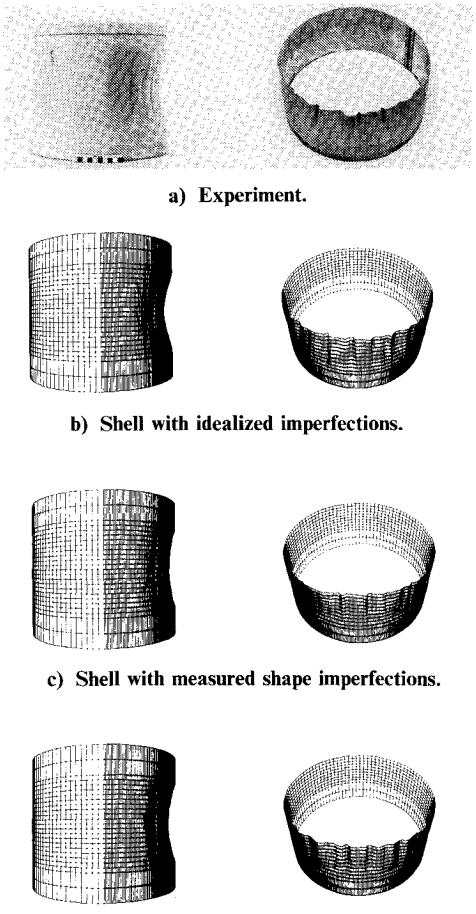

a) Experiment.

b) Shell with idealized imperfections.

c) Shell with measured shape imperfections.

d) Shell with measured shape imperfections and estimated load imperfections.

Fig. 10 Deformed shape of shells; calculations shown at 600 μs.

nearly identical to the calculations using the 1024- and 512-element meshes (Figs. 8a and 8b).

Sensitivity to Initial Imperfections

Six ring calculations were performed to investigate the effect of imperfections on the buckling response. The imperfections for the first calculation were generated using Eq. (1) for the estimated imperfections with a first set of random modal phase shifts. The deformed shapes at 120 and 600 μs for the ring with this first set of idealized imperfections are shown in Fig. 9a.

To determine the effect of the amplitude of the imperfections on the buckling response, we generated two more sets of imperfections. These imperfection distributions had the same set of random modal phase shifts, but the amplitude of the imperfections was increased by an order of magnitude for the first set and decreased by an order of magnitude for the second set. The deformed shapes for the larger and smaller imperfection sets are shown in Figs. 9b and 9c, respectively.

Comparison of these three calculations shows that the buckling is sensitive to order-of-magnitude changes in the amplitude of the imperfections. The deformed shape of the first ring at 120 μs shown in Fig. 9a appears to be the closest approximation to the experimentally observed response in Fig. 2.

A fourth set of estimated imperfections was generated using Eq. (1) with a new set of random modal phase shifts to study the effect of the random phase shift selection on the buckling. The deformed shape resulting from these new imperfections is shown in Fig. 9d. Comparison with the calculation using the first set of imperfections shows that, although the details of the buckling changed, the buckling threshold, mode number, and stress time histories of the response showed little change.

We performed two additional calculations on rings using the shape imperfections measured in the shell. Only the shape imperfections were included in the first calculation shown in Fig. 9e. The buckling response in this calculation is suppressed compared to the response of the ring with the idealized imperfections (Fig. 9a). The suppressed buckling response was expected because of the relative magnitude of the measured and idealized imperfections shown in Fig. 5. The second calculation included both the measured shape imperfections and the estimated imperfections in the load distribution. The calculated buckling response shown in Fig. 9f is more pronounced than the buckling response of the measured imperfections alone (Fig. 9e), but still suppressed in comparison with the response of the ring with the idealized imperfections (Fig. 9a).

After comparing the measured shapes of the ring in the flash x-ray experiment with the calculated shapes, we conclude that both of the idealized shape imperfections lead to a response similar to that observed in the experiments, although the details of the calculation vary with the set of random phase angles. The measured shape imperfections alone result in a suppressed buckling response compared to the experiment. The measured shape imperfections with the estimated load imperfections give better agreement with experiment. (Calculations with only the load imperfections did not show significant buckling.)

Calculation of Shell Response

We made three calculations predicting the shell response shown in Fig. 3. We used the idealized imperfection distribution in the first calculation without any load imperfections. The second and third calculations used the measured shape of the shell, first without any load imperfections and then with idealized load imperfections.

The finite-element models used to calculate the response of the shell used the symmetry at the midplane of the shell to reduce the size of the mesh by a factor of two. However, because of the random imperfections in the shell, no other plane of symmetry exists in these calculations. The shell meshes were generated with 200 elements around the front half of the shell and 50 elements around the back half of the shell. The models had 10 elements along the 7.6-cm half-length of the unsup-

ported test region and 2 elements along the 5.1-cm end ring, yielding a total of 3000 elements. The load produced by the MDF was approximated by a step followed by an exponential decay with a characteristic time of 30 μs. The peak impulse intensity at the 0 deg position was 210 Pa-s. All calculations were run for a 600-μs problem time, during which time the plastic deformation of the shell was completed.

The first shell calculation used the idealized shape imperfections defined by Eq. (1) and no imperfections in the load. The predicted shell response is shown in Fig. 10b, along with the corresponding photographs of the experiment, Fig. 10a. The views shown are a side profile and an oblique view of one-half of the shell. (The physical shell was cut in half after the experiment.) The buckling mode number in the calculation is approximately 40, corresponding well to the experimentally observed buckling mode number. To ease comparison between analysis and experiment, Table 1 compares several measures of response at the shell midplane: the dominant buckling mode numbers, the average inward deflection, the peak-to-peak amplitude of the buckles, the maximum inward deflection, and the axial strain. Because of the buckles, the magnitude of the axial strain in the shell will vary with the circumferential location. In this first calculation, the measured displacements are similar to the calculated values. They are well within the estimated accuracy of the experiment ($\pm$15%), which includes the uncertainty in impulse intensity and measurement error as well as the random effects of the buckles.

In the second shell calculation, we used the measured shape of the physical shell in generating the finite-element mesh, but did not include the imperfections of the load. If only the shell shape imperfections were important to response, the measured and predicted deformed shapes should be similar for this calculation. The deformed shape of the shell calculation at 600 μs is shown in Fig. 10c. In this calculation, the predicted buckling mode number is from 35 to 40, but the calculated shape does not correspond well to experiment. Comparison of the midplane responses given in Table 1 shows that the calculation underestimates the displacements by about 30%.

The third shell calculation included both the measured shape imperfections and the estimated imperfections in the load distribution calculated from Eq. (5). The predicted response of the shell is shown by the deformed finite-element mesh in Fig. 10d. In this calculation, the buckle mode number is again between 35 and 40. Table 1 gives the maximum peak-to-peak deflection at the shell midplane and other response parameters. This calculation shows better agreement between analysis and experiment than the second calculation, but not quite as good as that obtained with the first calculation. The errors in displacement are within the experiment accuracy.

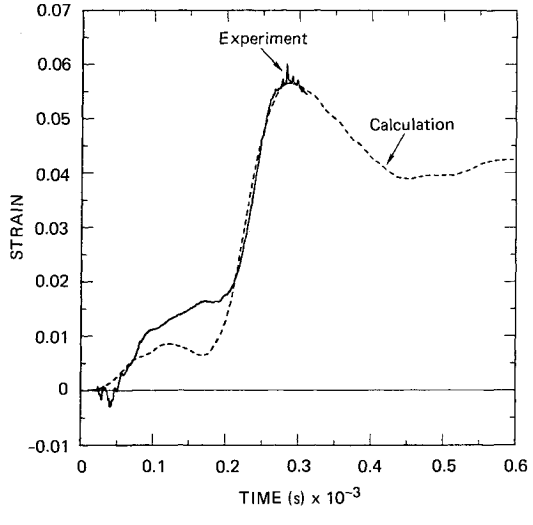

Fig. 11 Axial strain at the shell midplane.

For the third calculation, Fig. 11 shows both the calculated and measured axial strain histories at the shell midplane along the 0 deg position. The calculated and measured strains show the same features, indicating that the temporal history of the response was similar in the experiment and the calculation. The near-perfect agreement of the peak strains is fortuitous due to the variations in the strain magnitude that occur with respect to the buckling pattern.

Summary and Conclusions

Two experiments were performed in which a thin, unsupported aluminum ring and a cylindrical shell with fixed ends were subjected to an external impulsive load with a cosine distribution. Both the ring and shell showed pulse buckling on the loaded side with a buckle mode number of about 40. Displacements in both experiments were large, and measured strains in the shell experiment were about 6%.

Both the ring and shell experiments were modeled with the DYNA3D finite-element code using a four-node shell Hughes-Liu element. We found it necessary to include initial physical shell imperfections to precipitate the buckling. An initial mesh refinement study using a ring model showed that a good solution required at least 10 elements per anticipated buckle wavelength. In addition, the solutions obtained were sensitive to the distribution of imperfections in the shell. Order-of-magnitude changes in imperfection magnitude produced large changes in buckle amplitude.

Three calculations with a model of the shell were performed. The first calculation, with a randomly generated idealized set of imperfections, predicted the measured strains and displacements to within the experimental accuracy. A second calculation that used the imperfections measured in the shell predicted less deformation and resulted in poorer agreement with the experiment. A final calculation using the measured imperfections and an estimate of the imperfections in load again produced agreement within the accuracy of the experiment.

These experiments and calculations highlight the importance of including the correct initial imperfections in the calculation of the dynamic pulse buckling of thin shells. Changes in the initial shape and load distribution imperfections produced noticeable changes in the solution. The optimum situation when performing a dynamic buckling response calculation on a thin shell is to incorporate the actual imperfections in the shape and load distribution. These imperfections will vary with the manufacturing process of the shell and the loading technique used. However, determination of the actual imperfections for every buckling calculation is not practical. An alternative is to incorporate idealized shape imperfections based on available data for thin cylindrical shells. These generic imperfections produced reasonable results in this study and should be a good approach for many calculations.

A further requirement for buckling calculations is the use of a sufficiently fine finite-element mesh. Proper modeling of the buckling response appears to require at least 10 elements per buckle wavelength. An inherent danger in making dynamic buckling calculations is that, if too few elements are used, the buckling response will be suppressed. This risk is increased when performing calculations without supporting experiments.

References

[1]Lindberg, H. E. and Florence, A. L., "Dynamic Pulse Buckling: Theory and Experiment," Defense Nuclear Agency, Washington, DC, Rept. DNA 6503H, 1983.

[2]Hallquist, J. O. and Benson, D. J., "DYNA3D Users Manual (Nonlinear Dynamic Analysis of Structures in Three Dimensions)," Lawrence Livermore National Lab., Livermore, CA, Rept. UCID-19592, Revision 2, March 1986.

[3]Hughes, T. J. R. and Liu, W. K., "Nonlinear Finite Element Analysis of Shells: Part I. Three-Dimensional Shells," *Computer Meth-*

ods in Applied Mechanics and Engineering, Vol. 26, June 1981, pp. 331–362.

[4]Hallquist, J. O., Benson, D. J., and Goudreau, G. L., "Implementation of a Modified Hughes-Liu Shell into a Fully Vectorized Explicit Finite Element Code," *Procedures of the International Symposium on Finite Element Methods for Nonlinear Problems*, Univ. of Trondheim, Trondheim, Norway, 1985.

[5]Abrahamson, G. R. and Goodier, J. N., "Dynamic Plastic Flow Buckling of a Cylindrical Shell from Uniform Radial Impulse," *Procedures of the Fourth U.S. National Congress of Applied Mechanics*, Berkeley, CA, June 1962, pp. 939–950.

[6]Goodier, J. N. and McIvor, I. K., "The Elastic Cylindrical Shell Under Uniform Radial Impulse," *Journal of Applied Mechanics*, ASME Trans. 86, Series E, Vol. 31, June 1964, pp. 259–266.

[7]Lindberg, H. E., "Buckling of a Very Thin Cylindrical Shell due to an Impulsive Pressure," *Journal of Applied Mechanics*, ASME Trans. 86, Series E, Vol. 31, June 1964, pp. 267–272.

[8]Anderson, D. L. and Lindberg, H. E., "Dynamic Pulse Buckling of Cylindrical Shells Under Transient Lateral Pressures," *AIAA Journal*, Vol. 6, April 1968, pp. 589–598.

[9]Lindberg, H. E. and Murray, Y., "Calibration and Analysis of the SPLAT (Spray Lead at Target) Impulse Simulation Technique," Defense Nuclear Agency, Washington, DC, Rept. DNA 0000F, Nov. 1983.

[10]Prantil, V. C., Kirkpatrick, S., Holmes, B. S., and Hallquist, J. O., "Response of a Very Thin Shell Under an Impulsive Load," *Finite Element Methods for Plate and Shell Structures 2: Formulations and Algorithms*, Pineridge Press Ltd., Swansea, U.K., 1986.

[11]Arbocz, J. and Babcock, C. D., "The Effect of General Imperfections on the Buckling of Cylindrical Shells," *Journal of Applied Mechanics*, ASME Trans., Vol. 36, March 1969, pp. 28–38.

[12]J. Arbocz, "The Imperfection Data Bank, A Means to Obtain Realistic Buckling Loads," in *Buckling of Shells, Procedures of a State-of-the-Art Colloquium*, Springer-Verlag, New York, 1982.

[13]Krieg, R. D. and Key, S. W., "Implementation of a Time-Dependent Plasticity Theory into Structural Computer Programs," *Constitutive Equations in Viscoplasticity: Computational and Engineering Aspects*, Vol. 20, ASME, New York, 1976, pp. 125–137.